Anal. Bioanal. Electrochem., Vol. 16, No. 1, 2024, 60-78
https://www.doi.org/10.22034/abec.2024.710595

Analytical & Bioanalytical Electrochemistry

Full Paper

Highly Sensitive Electrochemical Immunosensor for Ultra-Low-Level Detection of Interleukin-10 using A Cost-Effective Gold Nanoparticle-Modified Electrode

Amalesh Nanda, Thangapandi Kalyani, Hiranmoy Kotal, and Saikat Kumar Jana*

Department of Biotechnology, National Institute of Technology, Papum Pare-791113, Arunachal Pradesh, India

*Corresponding Author, Tel.: +91-9485230608
E-Mail: saikatmicro4@gmail.com

Received: 5 October 2023 / Received in revised form: 27 January 2024 / Accepted: 27 January 2024 / Published online: 31 January 2024

Abstract- In developing countries, most women are suffering from endometriosis disease and unfortunately, there is not yet an efficient and adaptable biomarker that could be explored further for the diagnostics of endometriosis. In this direction, we are proposing interleukin-10 (IL-10) as a better biomarker and its efficient electrochemical immunosensing at an ultra-low level for the diagnosis of endometriosis based on demonstrated high sensitivity and specificity. To develop the proposed sensing platform, a glassy carbon electrode (GCE) was electrochemically modified with gold nanoparticles (AuNPs) utilizing the chronoamperometric method. Further, the Au/GCE platform was functionalized using a cysteamine-self-assemble monolayer through glutaraldehyde to achieve successful immobilization of the monoclonal IL-10 antibody and selective detection of IL-10 in real samples as well. The interaction between monoclonal IL-10 antibody and IL-10 antigen was studied using square wave voltammetry (SWV) technique. The cysteamine-based immunosensor displayed a dynamic range from 1 atto gram (ag i.e., 10^{-18} g) to 5 pico gram (pg i.e., 10^{-6} g) per mL, and the lower detection limit of 0.33 ag per mL of IL-10 was obtained. The validation of achieved sensing performance was evaluated by comparing all the parameters regarding the Enzyme-linked immunosorbent assays (ELISA). Additionally, the developed sensing platform exhibits high sensitivity, specificity, and reproducibility together with high stability and provides an effective appose to detect IL-10 cost and time-effective compared to ELISA. Thus, such AuNPs-based IL-10 sensing platforms of high-performance features can be promoted as an efficient analytical tool for clinical application to support women's healthcare globally.

Keywords- Endometriosis; IL-10 sensing; Gold nanoparticle; Biosensing; Diagnostics

1. INTRODUCTION

Endometriosis is an enigmatic gynecological disease that is the most upsurge women's health problem, approximately observed in 10-15% of women in their reproductive age. Endometriosis is a medical condition where there is the growth and spread of functional endometrial glands and tissue outside the uterus [1]. As a result, functional endometrial tissue is often found in various organs and tissues beyond its normal location, including the ovaries, abdominal cavity, pelvic organs, and occasionally in the bowel, ureter, bladder, or lungs [2]. Nowadays, endometriosis is a common gynecological women's health dysfunction that mostly leads to infertility in 15-25% of women at their childbearing age [1,2]. Apart from infertility, women are susceptible to suffering dysmenorrheal, dyspareunia, dysuria, dyschezia, chronic pelvic pain, and abnormal menstruation, all of which are usual syndromes during endometriosis [3–6]. The patients are affected by endometriosis due to the unknown etiology, inconsistent clinical manifestations, and difficult diagnosis, and the treatment is not standardized [2,7,8]. Previous studies have indicated that the pathogenesis of the disease is very complicated and involves mechanical, hormonal, immune, environmental, and genetic factors, but nothing is inconclusive [9–11].

Now it is established that T-lymphocytes and their related cytokines have a major role in disease development. Whereas the T-helper 1 (Th1) subset elevates the levels of pro-inflammatory cytokines such as TNF-α, IL-1β, IL-6, 12 and IFN-γ within the peritoneal fluid (PF) [12,13]and Th2 response to elevated levels of IL-4 and IL-10 within peripheral blood in women with endometriosis [14,15]. Besides, regulatory T-cells modulate the severity of the inflammatory response via the production of regulatory cytokines such as IL-10 and TGF-β1 [16]. Now, accumulating evidence has indicated that chronic inflammation and immune responses evoke a pivotal role in the development and growth of endometriosis. Moreover, numerous immunological biomarkers, including IL-2, IL-4, IL-6, IL-10, IL-11, IL-13, IL-17A, IL-37, IFN-γ and TNF-α, act as mediators that can accelerate the progression of endometriosis [17,18]. These cytokines have been suggested as important targets for endometriosis treatment or as non-invasive serum indicators for detection [19, 20]. Out of all those serum cytokines, it has been noted that IL-37 and IL-10 expression levels were noticeably greater in the endometriosis group than in the control group in the serum sample [17,21]. According to reports, the development and maintenance of endometriosis are significantly aided by increased expression of the multifunctional cytokine IL-10 [22]. In previous studies, multivariate statistical analysis was utilized to identify the key factor(s) involved in the pathogenesis of endometriosis, with a specific focus on IL-10. This analytical approach allowed researchers to determine the most critical factor related to the development and progression of endometriosis. [23]. According to previous work by Yan-Yan Fan [17], IL-10 has a higher sensitivity (92.59%) and specificity (100%) than IL-37 (81.48 and 83.33 percent), respectively. Many patients with endometriosis have suffered from ineffective non-invasive diagnostic methods and treatments,

which are frequently associated with multiple adverse effects and high rates of recurrence. Because of this, endometriosis has a serious influence on patients' quality of life, having a detrimental effect on their social and family lives as well as increasing healthcare costs [24,25].

The advancement of technology is crucial in enhancing sensor platforms that enable easy, sensitive, and direct measurement of levels of target biomarkers in clinical samples. There have been numerous standardized detection techniques for the diagnosis of endometriosis, including laparoscopy [26], ELISA [27,28], electro-chemiluminescence immunoassay, radioimmunoassay (RIA), fluorescence [26], piezoelectric [27,28], surface Plasmon resonance [29,30], and electrochemical techniques [31,32], Western blot [33,34] etc. but they are very imprecise in the prediction of the biological response. Apart from all the techniques, ELISA is very sensitive and accurate but time-consuming, requires proficient personnel, high cost, and requires a large amount (at least 5 ml) of sample for analysis. To overcome these challenges, a biosensor (an electrochemical immunosensor) with high sensitivity was developed specifically for detecting particular biomarkers [35] This electrochemical biosensor has profound advantages: being inexpensive, portable, easy to handle, fast, real-time analysis, less space-consuming, and reliable for quick medical diagnosis [36–38]. Gold nanoparticles provide a great platform for improving immunosensor performance because of their distinct electrical and chemical characteristics [39–42]. The best prognostic protein testing approach is connected with practical and financial issues.

Baek et al. reported a study on the detection of IL-10 using gold nanoparticles through the application of Localized Surface Plasmon Resonance (LSPR) [43]. Abdoullatif Baraket developed a prototype of an electrochemical micro-lab-on-chip system specifically designed for the detection of IL-10 [44]. Michael Lee and his team presented a capacitance biosensor that utilized hafnium oxide for the detection of IL-10 [45]. Abdoullatif Baraket et al. investigated the electrochemical immunosensor for the detection of IL-10 using the gold nanoparticle (AuNPs)-based sensing electrode. Here, the AuNPs electrode was functionalized with 16-mercapto hexadecenoic acid followed by carbodiimide chemistry [44]. Nanofilm semiconducting nanomaterial modified electrode for the detection of IL-10 in undiluted plasma samples reported by Ambolika S. Abdoullatif Baraket et al. also reported an integrated electrochemical sensing platform for the detection of IL-10 using gold microelectrodes [46,47]. A polypyrrole-modified silicon nitride-based electrochemical impedimetric immunosensor for the detection of IL-10 was reported by Faiza Nessark [48].

Considering the above discussion as motivation, this research reports a Cysteamine and AuNPs-modified GCE-based electrochemical immunosensor for sensitive, selective detection of IL-10 at a very ultra-low level (10^{-18} g). Careful and systemic studies were performed to fabricate a sensing platform and step-by-step sensing of the IL-10 biomarker using samples prepared in the lab and also in real samples. It demonstrated how the modified electrode could efficiently encourage the direct transfer of the probe $[Fe(CN)_6]^{3-/4-}$ to the electrode and

significantly raise the immunosensor's sensitivity. Additionally, this immunosensor demonstrated remarkable capabilities, including high sensitivity, strong selectivity, good stability, and repeatability. This strategy can be translated for the detection of IL-10 in clinical settings with support for women's health management.

2. EXPERIMENTAL SECTION

2.1. Chemical and instrumentation

All the chemicals were dispensed in analytical grade unless otherwise stated. Cysteamine (Cyst, C_2H_7NS, 98 %), Glutaraldehyde solution (Glu, $C_5H_8O_2$, 50 wt % in H_2O), bovine serum albumin (BSA, 96 %) were acquired from Sigma Aldrich, India. Sulphuric acid (H_2SO4), Hydrogen peroxide (H_2O_2), ethanol (C_2H_5OH, 99 %), potassium hydroxide (KOH, 98%), potassium nitrate (KNO_3), PBS tablet (pH- 7.4), potassium ferrocyanide ($K_4Fe\ (CN)_6$), potassium ferricyanide ($K_3Fe\ (CN)_6$) were purchased from HiMedia. Interleukin-10 antigen (IL-10, RPA066Hu02) and antibody (PA066Hu02) were bought from CloudClone Corp. Recombinant CA125 (5609-MU-050) was bought from R&D Systems. Recombinant carbohydrate antigen 19-9 (CA 19-9) (MBS2011087) and recombinant CEA(MBS142843) were bought from Mybiosource. Milli-Q water was used to prepare all of the solutions.

All electrochemical measurements were performed with a SP150 Bio-Logic Science Instrument (electrochemical workstation, France) that was coupled to a computer and controlled by EC Lab software. In order to conduct electrochemical studies, three-electrode systems were used: a platinum (Pt) auxiliary electrode, an Ag/AgCl reference electrode, and a glassy carbon electrode (GCE) as the working electrode. To determine the electrochemical characteristics of the alteration of GCE, cyclic voltammetry (CV), electrochemical impedance spectroscopy (EIS), and square-wave voltammetry (SWV) techniques were used. To perform these characterizations, $[Fe\ (CN)_6]^{3-/4-}$ was employed as an electroactive indicator at a concentration of 10 mM in a PBS solution with a pH of 7.4. For SWV, the optimal parameters used were a pulse height (PH) of 25 mV, a pulse width (PW) of 50 ms, and a step height (SH) of 10 mV. These parameters allowed for precise and effective characterization of the modification of the GCE.

2.2. Pre-treatment of glassy carbon electrode (GCE)

The GCE surface was immersed in a newly made piranha solution consisting of 30% H_2O_2 and concentrated H_2SO_4 in a volumetric ratio of 1:3. This step was performed to remove any organic residues present on the substrates. The immersion time lasted around 5 minutes. The GCE electrode underwent a washing and drying process using a nitrogen flow. Subsequently, mechanical polishing was performed on the electrode using an alumina slurry with particle

sizes of 1.0, 0.5, and 0.3 µm. The electrode was then subjected to sonication in distilled water and 100% ethanol for a duration of 15 minutes each, in order to eliminate any remaining alumina powder. Subsequently, the electrode underwent electrochemical cleaning by utilizing CV in a 0.1 M H_2SO_4 solution. The experimental setup involved applying a potential window spanning from -0.2 V to 1.6 V, with a scan rate of 0.1 V/s, over a total of 10 cycles. Subsequently, the electrode underwent sequential rinsing with Milli-Q water and ethanol, followed by drying with a dry N_2 flow.

2.3. Fabrication of immunosensor

Scheme 1 depicts the gradual modification of the surface of a label-free electrochemical immunosensor. The electrochemical modification of a pre-treated GCE electrode was accomplished by dipping it into a solution of $HAuCl_4.3H_2O$ (6 mmol L^{-1}) containing 0.1 mol L^{-1} KNO_3 as a supporting electrolyte. After that, Au nanoparticles were electrodeposited using cyclic voltammetry with a cathodic potential sweep of -0.2 to -1.2 V for 20 cycles in an N_2 environment. By repeatedly depositing nanoparticles on the polycrystalline GCE electrode, the electrochemical surface area was enhanced. On gold nanoparticle-modified electrode (AuNPs/GCE), self-assembled monolayers (SAM) of Cyst were formed. In that instance, the AuNPs/GCE electrode was dipped for 16 hours at 40^{o}C in a 10 mM per mL ethanolic solution of Cyst. Following this, unbound Cyst residues were removed from the Cyst/AuNPs/GCE by rinsing with 100% ethanol and water, respectively, and drying under a dry N_2 flow. The Cyst/AuNPs/GCE electrode's terminal amino groups were then used for activation and additional modification by submerging the electrodes in a 2.5% Glu solution for 60 min. This resulted in the formation of a cross-linked monolayer on the SAM-modified AuNPs/GCE. The resultant electrode was then repeatedly rinsed in PBS buffer (pH 7.4) to eliminate any loose Glu connections. After that, the Glu/Cyst/AuNPs/GCE electrode was immediately incubated for 40 minutes at room temperature with a solution of 10 g mL^{-1} anti-IL-10 (IL-10 antibody) in PBS (pH 7.4) before being washed with PBS. To block potential remaining active sites of the nano-Au monolayer and prevent non-specific adsorption, the modified immunosensor (IL-10ab/Glu/Cyst/AuNPs/GCE) was lastly incubated in 1% BSA solution for roughly 30 min at 25^{o}C. To prevent unbound absorption, a thorough PBS wash was performed on the acquired electrode. The immunosensor that was finally obtained (BSA/IL-10ab/Glu/Cyst/AuNPs/GCE) was prepared for sensing and measuring IL-10 antigen using the techniques listed below. The resultant BSA/IL-10ab/Glu/Cyst/AuNPs/GCE electrode was incubated for 40 minutes at 25^{o}C with 1 pg mL-1 Il-10 antigen, which was diluted from a stock solution of 1000 ng. mL^{-1} IL-10 to the appropriate concentration.

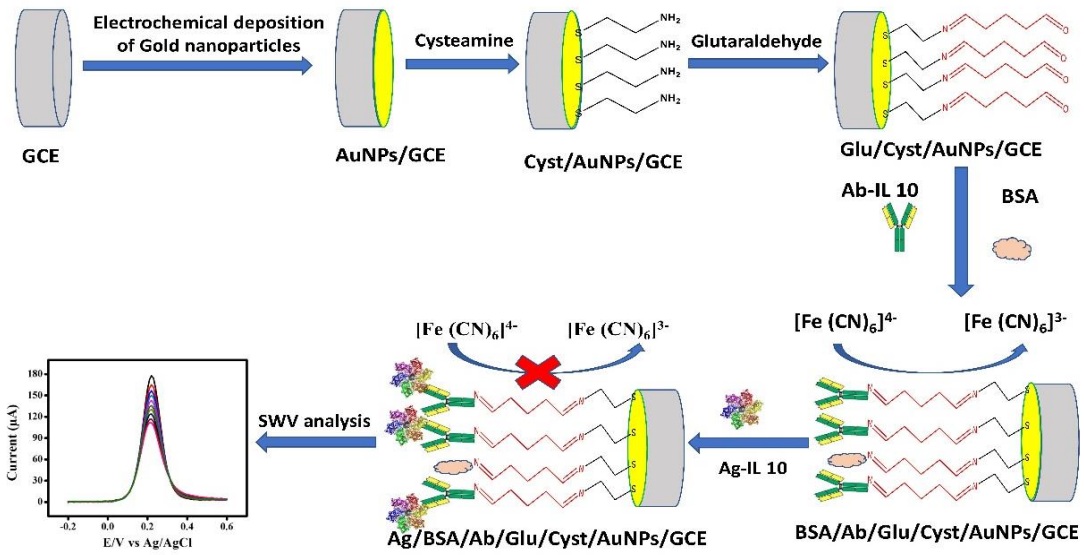

Scheme 1. A schematic diagram illustrating the process of fabricating a modified electrode and detecting IL-10

2.4. Blood sample collection

Veteran gynecologists recruited both healthy and endometriotic women for the study. The study on women's health, conducted at the National Institute of Technology in Arunachal Pradesh, India, was approved by the Science and Engineering Study Board (SERB) of the Department of Science and Technology (DST). To ensure ethical compliance, permission was obtained from the institutional scientific ethics council with Proposal Number: NIT (A.P)/R&D/Project/11-12/1/Vol.2/IEC-02, approved on 27/09/2016. Participants in the study provided written consent before their blood samples were collected. Before commencing the research, necessary approvals were obtained from the Pratiksha Hospital in Guwahati, Assam, and the Indian government. Participants in the trial had not received any hormonal or pharmaceutical therapy in the three months before. Women who had undergone abdominal surgery, lower pelvic pathology, such as pelvic TB, or any gynecological surgery in the past were also disqualified from the trial. Each participant freely and voluntarily provided their consent. As stated previously, various blood samples were collected.

2.5. Sample preparation for Characterization

Indium tin oxide (ITO) plate was initially cleaned and pretreated to remove any impurities or contaminants. Then Gold nanoparticles were electrodeposited onto the cleaned ITO surface using cyclic voltammetry technique with a cathodic potential sweep of -0.2 to -1.2 V for 20 cycles. After the AuNP deposition, the modified electrode was allowed to dry at room temperature. Then the AuNPs are removed from the ITO surface gently and mixed with absolute alcohol.

3. RESULTS AND DISCUSSION

3.1. Characterization of AuNP-modified GCE

To get the ideal size and distribution of AuNPs on the GCE for enhancing analytical performance, the gold deposition time was assessed. Figure 1A depicts SEM images of AuNPs located on GCE. This suggests the successful deposition of AuNPs onto the glassy carbon surface. The results of the TEM (Figure 1C and D) analysis showed that the AuNPs had a uniform distribution and had an average size of 28.8 nm.

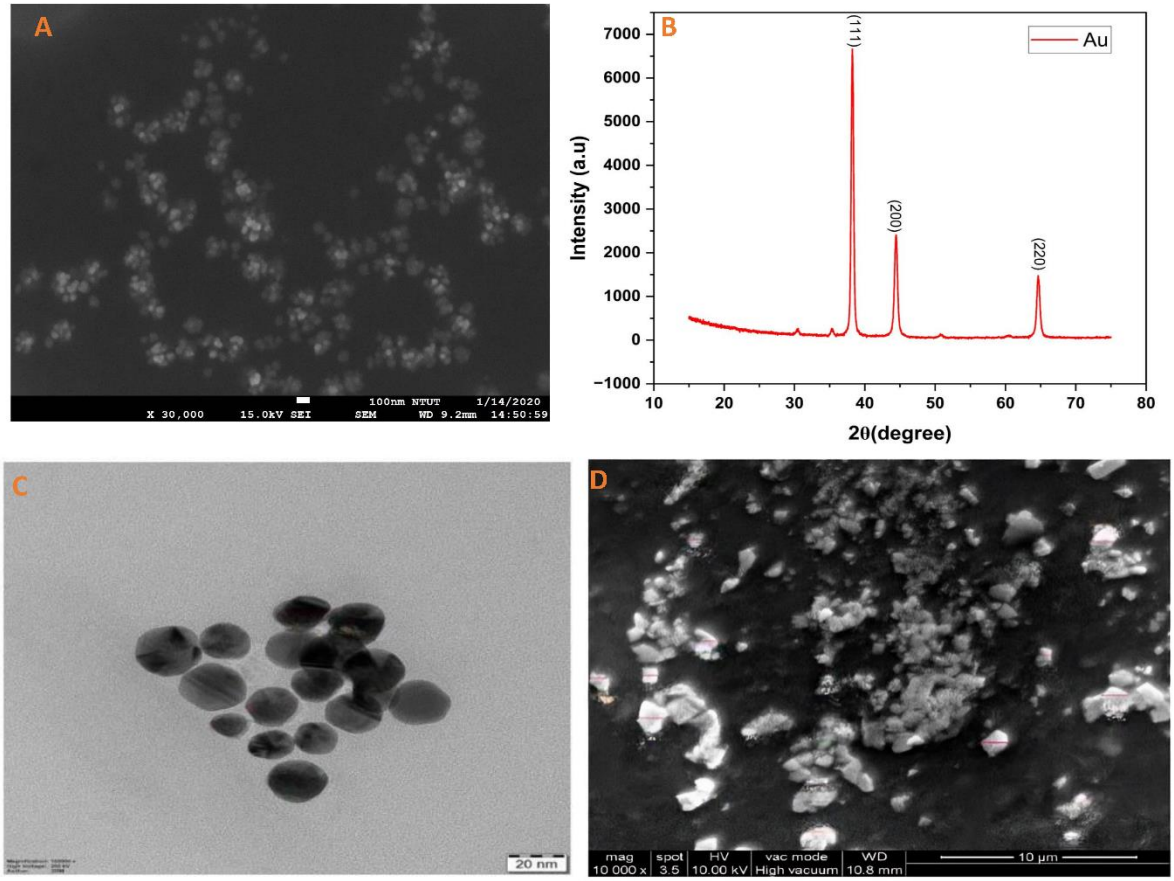

Figure 1. (A) SEM image of electrodeposited AuNPs; (B) XRD diffractogram of AuNPs, lines denote gold crystalline planes; (C&D) TEM image of electrodeposited AuNPs

X-ray diffraction (XRD) was used to analyze AuNPs, and the related XRD patterns are depicted in Figure 1B. Three different peaks were visible in gold nanocrystals at 2θ = 38.2, 44.4, and 64.6. The three peaks were identical to the face center cubic (fcc) lattice's conventional Bragg reflections (111), (200), and (220). The investigation reveals that the AuNPs in the sample are polycrystalline, with the highest diffraction peak observed at 38.2. This finding suggests that a significant portion of the AuNPs in the sample predominantly exhibit the Au (111) phase.

3.2. Electrochemical characterization

The surface modification of the electrode is a crucial step that greatly influences the efficiency and performance of the immunosensor in the future. After preparing the immunosensor, CV and EIS techniques were used to demonstrate the stepwise construction approach of the proposed immunosensor utilizing $[Fe(CN)_6]^{3-/4-}$ as a standard redox marker. Consequently, a standard redox probe consisting of 10mM $[Fe(CN)_6]^{3-/4-}$ and 1 M KNO_3 in PBS (pH 7.4) was utilized. The potential range for the probe was set from -0.2V to 0.6V, with a scanning rate of 0.02V/s. In Figures 2A and 2B, the cyclic voltammetry (CV) response and electrochemical impedance spectroscopy (EIS) spectra illustrate the gradual construction of the immunosensor in 0.1M KCl/10mM $[Fe(CN)_6]^{3-/4-}$ respectively. The anodic peak potential (E_{pa}) of the bare GCE was +0.276 V, while the cathodic peak potential (E_{pc}) was +0.195 V and the oxidative peak current was 0.221 mV. Regenerate response After gold nanoparticle modification, the peak current of AuNPs/GCE was significantly increased (*I*=0.268 mV) compared with a bare electrode (black). The observed effect can be attributed to the capability of AuNPs to enhance electron transfer between electroactive species and electrode substrates. This indicates that the combined platform has the potential to substantially improve the sensitivity of the immunosensor. Additionally, the AuNPs can enhance the effective electrode surface area, which may allow for the attachment of additional antibodies, thus amplifying the signal. After Cyst modification, Cyst/AuNPs/GCE was compared with AuNPs/GCE, and the resulting peak current was reduced (*I*=0.252 mV, sky blue color). These results consisted of coverage of the electrode surface by insulating a self-assembled monolayer (SAM). Bi-functional cross-linker Glu was introduced with Cyst layers. Each molecule of Cyst has two amino groups; antibodies with amino groups can be bound to GCE by cross-linking with Glu. As a result, the SAM is attached to the gold electrode surface by the thiol group. Figure 2A showed that the peak current (*I*=0.241 mV, shown in pink) was lower than that of Cyst/AuNPs/GCE (shown in sky blue). This observation demonstrated that the Glu was successfully attaching to the Cyst layer. Next, the Glu/ Cyst/ AuNPs/GCE was incubated with anti-IL-10. Again, the current (green color) was lowered as a result of antibody binding with Glu (*I*=0.230 mV). Glu reacts with lysine residues on the antibody to generate Schiff base bonds. The IL-10Ab/Glu/Cyst/AuNPs/GCE was incubated in 1% BSA to prevent nonspecific binding to the active electrode surface. As a result, the peak current (blue color) was reduced (*I*=0.218 mV). Finally, IL-10 antigen was incubated with BSA/IL-10Ab/Glu/Cyst/AuNPs/GCE. Due to the formation of an antigen-antibody immunocomplex with a nonconductive nature, the peak current (purple hue) decreased continuously (*I*=0.209 mV). Additionally, using the CV approach, the electrochemical scan rate investigation of the BSA/IL-10Ab/Glu/Cyst/AuNPs/GCE bioelectrode was examined at various scan rates ranging from 10 mV s^{-1} to 100 mV s^{-1} (Figure S1).

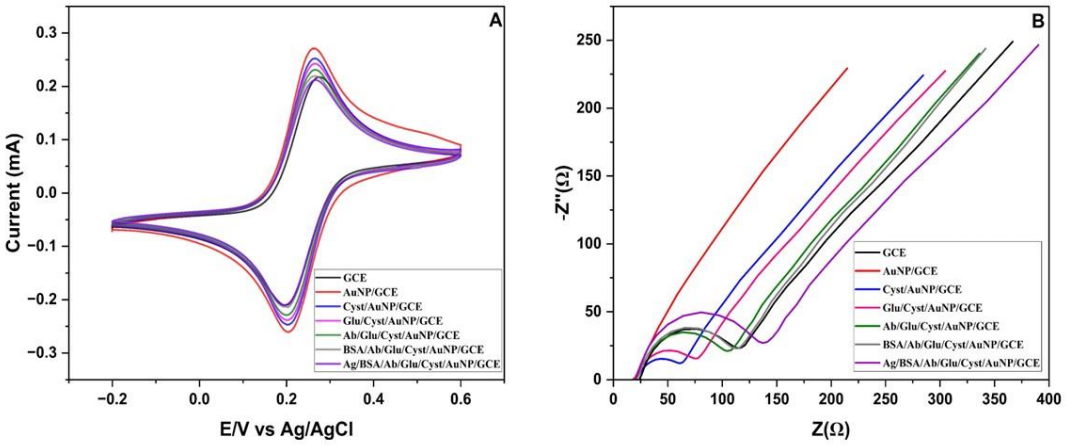

Figure 2. CV (A) and EIS (B) response of the step-by-step construction of immunosensor in 0.1M KCl/10mM [Fe $(CN)_6]^{3-/4-}$, bare GCE (black), AuNP/GCE (red), Cyst/AuNP/GCE (blue), Glu/ Cyst/AuNP/GCE (pink), Ab/Glu/Cyst/AuNP/GCE (green), BSA/ Ab/Glu/Cyst/AuNP/GCE (gray) and Ag/BSA/Ab/Glu/Cyst/AuNP/GCE (purple), respectively

An efficient method for examining the characteristics of electrodes with surface modifications is electrochemical impedance spectroscopy (EIS), which also provides more proof of the impedance during the immobilization process. Additionally, the nature or spectroscopic curve characteristics of EIS were used to infer the equivalent circuit's structure [49]. The impedance spectra exhibit two primary constituents: a semi-circular segment that signifies the resistance encountered during electron transfer, and a linear segment that represents the diffusion-limited process. The presence of smaller curved semicircles results in a decrease in resistance, hence facilitating the process of charge transfer. These semicircles within the EIS curve reveal the interface layer resistance occurring on the electrode surface. In 0.1 M KCl aqueous solution containing 5 mM $[Fe(CN)_6]^{3-/4-}$, the electron transfer of the unmodified GCE (a) and modified AuNP/GCE (b) electrodes was examined, and it was depicted in Figure 2B. The electron transfer resistance (R_{ct}) in series with the parallel connection of the Warburg impedance (Z_w) and double layer capacitance (C_{dl}) results in the total electrode impedance. The bare GCE electrode (black color) showed a R_{ct} Value of 90.42 Ω and the AuNPs-modified AuNPs/GCE electrode (red color) displayed a near-linear response which suggests that the gold electrode facilitated the rate of electron transfer of the redox marker at the electrode surface. The semi-circular diameter of SAM-modified GCE (blue color) was larger (Rct value: 38.91 Ω) than AuNPs/GCE (red color) when AuNPs/GCE was absorbed with a cysteamine molecule. This finding elucidates the related blocking effect of the SAM layer on charge transfer. Similarly, increasing R_{ct} values at each stage validate the blocking effect of the redox probe towards the electrode surface after SAM-modified electrode surface modification with glutaraldehyde (pink, R_{ct} value: 54.22 Ω), anti-IL-10 antibody (green, R_{ct}

value: 81.9 Ω), BSA (gray, R_{ct} value: 88.37 Ω), and IL-10 (purple, R_{ct} value: 116.02 Ω), which was compatible with the CV result.

3.3. Optimization step of immunosensor

Many factors interfere in the development as well as in the performance of electrochemical immunosensors. Wherein, the incubation temperature and time for the immune reaction, the concentration of Ag-Ab, and the pH value of the substrate solution were the highest impact. So, the efficiency of the proposed immunosensor was enhanced by optimization through experimental values of the intervention factors.

3.3.1 Optimization glutaraldehyde incubation time

The glutaraldehyde optimization on Cyst/AuNP/GCE has been done by different incubation periods. Figure 3A demonstrates that the resulting peak current decreased simultaneously with an increase in the incubation time of glutaraldehyde. In this study, different time of incubation was applied ranging from 1-120 min (1, 5, 10, 20, 40, 60, 80,100, and 120). The peak current was almost constant after 60 min incubation which implies optimization has been done completely due to Glu saturation on the electrode. Hence, 60 min incubation time was selected for the immunosensor.

3.3.2. Optimization of anti-IL-10 incubation time

The incubation time of anti-IL-10 was found to be a crucial factor in the response of the developed immunosensor. The immunosensor was tested for various durations, ranging from 0 to 60 minutes (0, 10, 20, 30, 40, 50, 60 minutes), using a 2µg/mL solution of anti-IL-10 (Figure 3B). The peak current measured by SWV decreased proportionally as the incubation time increased from one minute to 40 minutes, which can be attributed to the non-conductive binding of antibodies on the glassy carbon electrode (GCE). However, after 40 minutes, the peak current of SWV remained constant, indicating that a further increase in the incubation time did not significantly affect the results. Hence, 40 minutes was concluded for the optimum incubation time of the antibody on the electrode surface.

3.3.3. Optimization of anti-IL-10 concentration

Different concentrations of anti-IL-10 incubation were also intensely influenced by the assessment of the proposed immunosensor and its stability. Figure 3C shows IL-10 antibody concentrations and the respective peak current of SWV. The peak current was reduced simultaneously when the IL-10 antibody concentration was increased from 2 to 16 µg/mL at 25ºC. This happened due to the immobilization of anti-IL-10 on the electrode surface. As a consequence, after some time, the peak current seems to be constant, further increasing the antibody concentration. Now the result suggests the electrode was saturated at a particular

concentration. Therefore, based on the findings, an antibody concentration of 14 µg/mL was determined to be the optimal concentration for constructing the immunosensor.

3.3.4. Optimization of blocking agent incubation time

Following the successful immobilization of anti-IL-10, the electrode was subjected to incubation in a 1% BSA solution with a pH of 7.4, prepared in 0.01 M PBS. The incubation time was varied, ranging from 0 to 60 minutes in intervals of 10 minutes (0, 10, 20, 30, 40, 50, and 60 minutes). During the initial 40 minutes of incubation, a noticeable decrease in the peak current of SWV was observed, as depicted in Figure 3D. This decline in peak current can be attributed to surface saturation. After the 40-minute mark, the SWV peak current remained constant, indicating that the maximum amount of BSA had been successfully immobilized on the electrode surface. Based on this data, it can be inferred that a 40-minute incubation period ensured the optimal immobilization of BSA on the electrode surface.

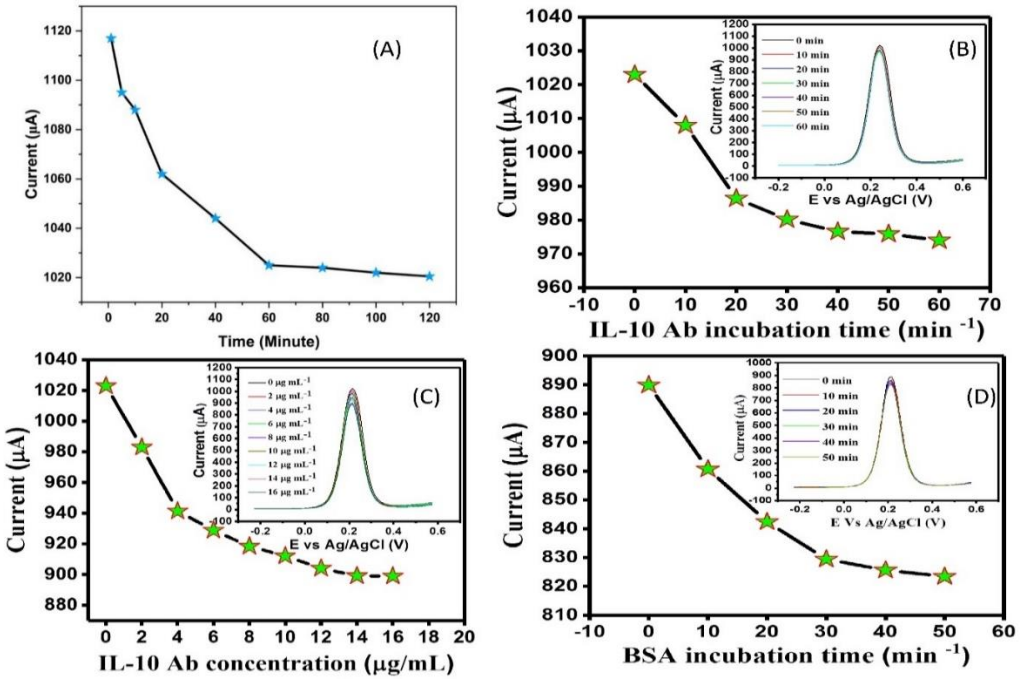

Figure 3. Optimization process for the following parameters in a 10 mM PBS solution containing 10 mM $[Fe(CN)_6]^{3-/4-}$ and 1 M KNO_3 solution: A. Glutaraldehyde incubation time B. Antibody incubation time C. Antibody concentration D. BSA incubation time

3.3.5. Optimization of incubation temperature & pH

The influence of temperature on the performance of the proposed immunosensor was investigated within a range of 10-50ºC, as illustrated in Figure S2A. The maximum response current was recorded at 35ºC, which remained unchanged up to 50ºC. The signal response had decreased drastically over 45ºC, possibly due to the thermal degradation of Ag and Ab. The results indicated that the most favorable temperature for the Ab-Ag interaction was 35°C.

The pH of the detection solution has a clear impact because the acidity of the solution may have an impact on the activity of the immobilized protein. The immunosensors were tested in a series of PBS buffers with pH values ranging from 6.0 to 9 by CV to optimize the pH value. The impact of detecting solution pH on the relative change in peak current is depicted in Figure S2B. When the pH of the solution rises from 6.0 to 9, the peak current increases until pH = 7.4, at which point it decreases due to the loss in protein activity. The ideal pH for this encounter is therefore chosen to be pH = 7.4.

3.3.6. Optimization of immune-reaction time

The effect of incubation time has a great impact on the response of the proposed immunosensor. For effective sensor development, a series of data has been recorded based on different incubation times and immunoreactions. Therefore, 10ng/mL of IL-10 solution was incubated at the last modified electrode for 10, 20, 30, 40, 50, and 60 minutes at 25°C. According to Figure S3, the peak current of SWV dropped proportionally with an incubation time of up to 50 minutes. This indicates that the immobilized anti-IL-10 completely interacted with the IL-10 antigen molecules. Even when simultaneously lengthening the incubation period, the peak current of SWV remained unchanged. Therefore, the best scenario for a longer incubation period of antigen and antibody was 50 minutes.

3.4. Analytical performance of the immunosensor

Under identical experimental conditions, the electrochemical performance of the recommended immunosensor (BSA/IL-10Ab/Glu/Cyst/AuNPs/GCE) was evaluated at various IL-10 concentrations. The response of the developed immunosensor decreased proportionally with increasing IL-10 antigen concentration (Figure 4A) due to the blockage of electron transport on the electrode surface, indicating that the anti-IL-10 antibody successfully captured the antigen.

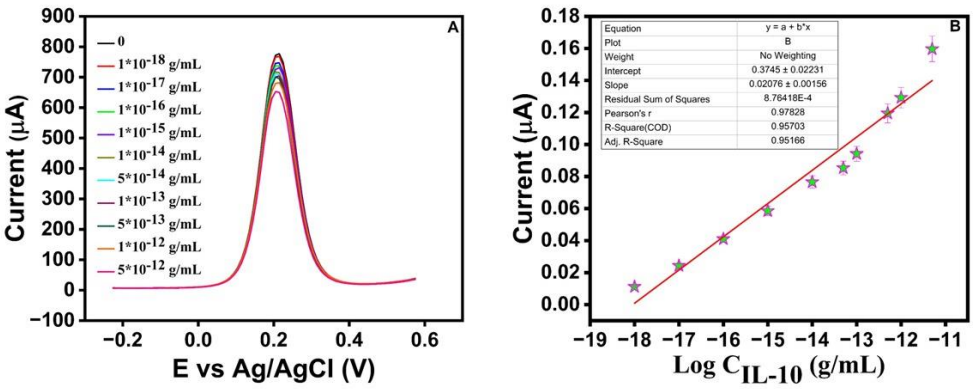

Figure 4. (A) SWV response of various concentrations of IL-10 ranging from 1 ag to 5 pg/mL, (B) Linear plot of the logarithmic concentration of IL-10 against the corresponding current

The anodic peak current reduction (I_pR (%)) was employed to obtain the IL-10 calibration curve. I_pR was calculated with the equation:

$$I_pR = [1-(I_p/I_p^0)] \quad (1)$$

In this equation, the peak current intensity Ip^0 and Ip of $Fe(CN)_6^{3-/4-}$ were indicated before and after the incubation with IL-10, respectively. Thereafter, the calculated current was changed linearly between the inhibition ratio ($(I^0 – I)/I^0$) of peak current and logarithm of IL-10 concentrations in a range from 1 ag/mL to 5 pg/mL with a detection limit of 0.33 ag/mL (S/N = 3) (Figure 4B). The linear regression equations were $(I_p^0–I_p)/I_p^0 = 0.3745 [\log_{IL\text{-}10}] + 0.02231$, with a correlation coefficient of $R^2 = 0.95703$.

Table 1. The analytical characteristics of the electrodeposited AuNP-based immunosensor were compared to those of existing immunosensors reported for IL-10 detection

S.No	Sensing platform	Methods	Liner rang	LOD	Reference
1	hafnium oxide (HfO_2)	EIS	0.1 pg/mL and 50 ng/mL	0.49 ng/mL	[45]
2	Polypyrrole (PPy)-modified silicon nitride (Si_3N_4)	EIS	1-50 pg/mL	0.347 pg/mL	[48]
3	Gold microelectrodes	EIS	1–15 pg/mL	0.47 pg/mL	[46]
4	AuNC and Au LSPR strip	Localized surface plasmon resonance (LSPR)	0.2 to 200 nM	0.06 nM	[43]
5	PAMAM decorated electrospun polystyrene fibers	CV&EIS	1-50 pg/mL	1 pg/mL	[50]
6	AuNP modified GCE	SWV	1 ag/mL to 5 pg/mL	0.33 ag/mL	This work

*LSPR- Localized surface plasmon resonance, AuNC-Gold nanocube, PAMAM- polyamidoamine

Table 1 presents a comparison of the analytical performance between the AuNP-based immunosensor developed in this study and other previously described immunosensors for the detection of IL-10. This study is the first to detect IL-10 using electrodeposited AuNPs as an interface, and its LOD is quite low. The main benefit of immunosensors is that they don't need expensive secondary antibodies or enzymes. The use of functionalized nanomaterials to enhance signals has also lowered the cost of making them.

3.5. Selectivity, reproducibility, stability, and regeneration of the immunosensor

Some contrast experiments were performed to investigate the specificity and legibility of the proposed immunosensor. The clinical sample analysis was a major hindrance for

immunosensor due to the numerous compound matrix forms [51]. The non-specific adsorption on the electrode surface was restricted by employing excellent selectivity. For the evidence, the immunosensor was introduced with specific IL-10 biomarker and non-specific biomarkers CA125, CA19-9, CEA shown in (Figure 5A). The resultant peak current was nearly identical to that of the control, presumably as a consequence of unbound molecules remaining on the electrode surface. Due to interfering biomarkers, a minor variance in SWV signal response was observed. The relative standard deviation (RSD) of the SWV reaction of the sample containing the interfering substance was less than 1%. This outcome shows that the immunosensor has good selectivity.

The reproducibility of the immunosensor was endorsed by a series of five electrodes for the detection of 1 pg/ml IL-10 under previously optimized experimental conditions (Figure 5B). The results elicited acceptable reproducibility and accuracy, with a relative standard deviation (RSD) of 1.8%, which reveals the good precision and accuracy of the sensor.

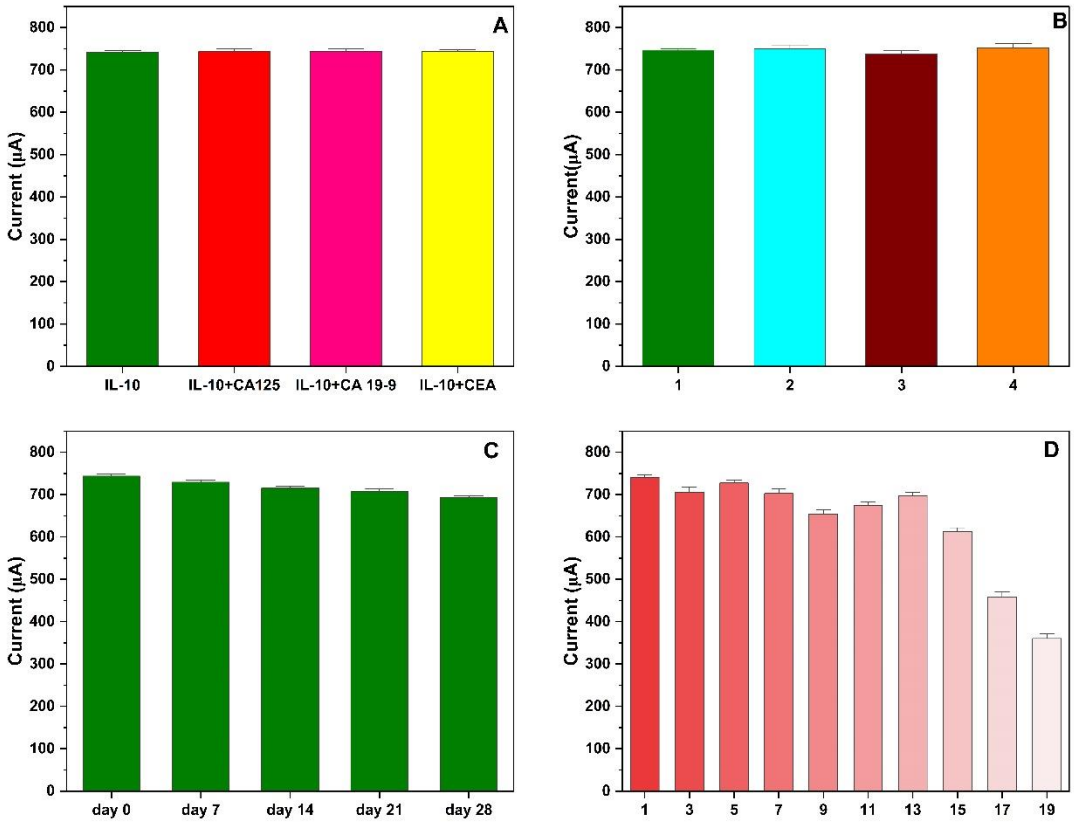

Figure 5. (A)The current response of fabricated immunosensor in the presence of 1 pg mL^{-1} IL-10, 1 pg mL^{-1} IL-10+ 10 U mL^{-1} CA 125, 1 pg mL^{-1} IL-10 + 10 U mL^{-1} CA 19-9, 1 pg mL^{-1} IL-10 + 100 pg mL^{-1} CEA, (B) SWV response of corresponding reproducibility, (C) SWV response for stability (D) SWV response of corresponding regeneration of immunoelectrode (1 pg mL^{-1} IL-10); all measurements were repeated three times (n = 3).

The stability of the proposed immunosensor was also investigated by periodic current measurement of 1 pg/ml IL-10. Finally, the modified electrode was stored in a refrigerator at 4^{o}C for 28 days in a 0.05 M PBS buffer. The stability and sensitivity of the immunosensor were examined every seven days intervals. The current response of the pre-developed immunosensor retained about 93.3% of the initial response value (Figure 5C).

The regeneration of the BSA/IL-10Ab/Glu/Cyst/AuNPs/GCE immune-electrode was displayed in Figure 5D. The attached IL-10 was dissociated from the bioelectrode to regenerate again for IL-10 rebinding. Experimental results indicated that the immunosensor could maintain 82.6% of the initial current response after being regenerated 15 times. The findings suggest that the immunosensor developed in this study demonstrates a high degree of reusability.

3.6. Analysis of Real sample

The fabricated immunosensor was analyzed to estimate real samples containing specific biomarkers. For analytical reliability and possible practical application, the developed immunosensor was used for quantitative and qualitative estimation of IL-10 in endometriosis serum samples. Primarily, the different stages of endometriosis had been reconfirmed depending upon the estimated concentration of IL-10 in serum, compared with the control sample. The diluted (100 times with PBS buffer pH 7.4) serum samples were analyzed by the proposed immunosensor. The results of the experiment were compared with those obtained using an enzyme-linked immunosorbent assay (ELISA) method, and the findings are shown in Table 2.

Comparing the experimentally obtained results, there is no significant difference between the two approaches, demonstrating a high correlation between ELISA and this suggested method. The average RSD value was observed at 1.664% and 2.026% for the proposed sensor and ELISA assay respectively. The result suggests that the proposed immunosensor is reliable for IL-10 detection.

Table 2. Electrochemical detection of IL-10 in endometriosis serum and parallel comparison with ELISA method

Source	**Proposed sensor**		**ELISA**	
	Found (pg mL^{-1})	**Std. dev. (n=3)**	**Found (pg mL^{-1})**	**Std. dev. (n=3)**
Healthy human	17.57	0.506	17.27	0.6701
Stage -I	77.11	0.9006	80.01	1.151
Stage -II	88.7	1.188	88.89	1.37
Stage -III	99.25	1.465	100.49	1.384
Stage -IV	134.32	1.82	136.55	1.989

4. CONCLUSION

In this investigation, we propose an electrochemical sensing platform based on AuNPs-modified GCE for IL-10 biomarker detection. Here, a cysteamine-self monolayer facilitated by glutaraldehyde was used to successfully immobilize monoclonal IL-10 antibody on the AuNP/GCE surface. Finally, the SWV technique was used to perform electrochemical analysis of the IL-10 antigen. The constructed immunosensor showed linear detection from 1 ag to 5 pg mL^{-1}, with a LOD of 0.33 ag mL^{-1} of IL-10. A high degree of selectivity, sensitivity, specificity, repeatability, and stability was also demonstrated by the electrochemical response current, demonstrating the superiority of the sensing platform. We believe that this extremely sensitive and selective approach has the potential to be used in clinical applications in light of the aforementioned benefits.

Acknowledgments

The study received financial support from the Department of Biotechnology, New Delhi, India, under the reference number BT/PR16930/NER/95/355/2015, dated 29 March 2017.

Declarations of interest

The authors do not have any conflicts of interest to disclose that are related to the subject matter of the study.

REFERENCES

[1] V.S. Counseller, American Journal of Obstetrics and Gynecology 36 (1938) 877.
[2] V.L. Kodati, S. Govindan, S. Movva, S. Ponnala, and Q. Hasan, Medical Hypotheses 70 (2008) 239.
[3] I. Ugo, and F. Barbieri, European Journal of Obstetrics & Gynecology and Reproductive Biology 150 (2010) 76.
[4] M. Cozzolino, M.E. Coccia, G. Lazzeri, F. Basile, and G. Troiano, Revista Brasileira de Ginecologia e Obstetrícia 41 (2019) 170.
[5] A.L. Hsu, N. Sinaii, J. Segars, L.K. Nieman, and P. Stratton, Obstetrics and Gynecology 118 (2011) 223.
[6] A.S. Laganà, V.L. La Rosa, A.M.C. Rapisarda, G. Valenti, F. Sapia, B. Chiofalo, and S.G. Vitale, International Journal of Women's Health 9 (2017) 323.
[7] L.M. Mikhaleva, V.E. Radzinsky, M.R. Orazov, T.N. Khovanskaya, A.V. Sorokina, S.A. Mikhalev, S.V. Volkova, V.B. Shustova, and M.Y. Sinelnikov, International Journal of Women's Health 13 (2021) 525.
[8] H. Malvezzi, E.B. Marengo, S. Podgaec, and C. D.A. Piccinato, Journal of Translational Medicine 18 (2020) 1.

[9] P. Viganò, F. Parazzini, E. Somigliana, and P. Vercellini, Best Practice & Research Clinical Obstetrics & Gynaecology 18 (2004) 177.
[10] Y. Wang, K. Nicholes, and I.M. Shih, Annual Review of Pathology: Mechanisms of Disease 15 (2020) 71.
[11] R. Hemmings, M. Rivard, D.L. Olive, J. Poliquin-Fleury, D. Gagné, P. Hugo, D. Gosselin, Fertility and Sterility 81 (2004) 1513.
[12] M. Tarokh, M. Ghaffari Novin, T. Poordast, Z. Tavana, H. Nazarian, M. Norouzian, and B. Gharesi-Fard, Iranian Journal of Immunology 16 (2019) 151.
[13] H. Chaudhry, J. Zhou, Y. I. N. Zhong, M.M. Ali, F. McGuire, P.S. Nagarkatti, and M. Nagarkatti, In Vivo 27 (2013) 669.
[14] S. Podgaec, M.S. Abrao, J.A. Dias Jr, L.V. Rizzo, R.M. De Oliveira, and E.C. Baracat, Human Reproduction 22 (2007) 1373.
[15] K. Szymanowski, J. Niepsuj-Biniaś, A. Dera-Szymanowska, M. Wołuń-Cholewa, A. Yantczenko, E. Florek, T. Opala, M. Murawski, and K. Wiktorowicz, BioMed Research International 2013 (2013).
[16] H. Hassa, H.M. Tanir, B. Tekin, S.D. Kirilmaz, and F. Sahin Mutlu, Archives of Gynecology and Obstetrics 279 (2009) 891.
[17] Y.Y. Fan, H.Y. Chen, W. Chen, Y.N. Liu, Y. Fu, and L.N. Wang, Gynecological Endocrinology 34 (2018) 507.
[18] V. Chopra, T.V. Ding, and E.V. Hanningan, Journal of Cancer Research and Clinical Oncology 123 (1997) 167.
[19] I. Flores, E. Waelkens, and T. D'Hooghe, Best Practice & Research Clinical Obstetrics & Gynaecology 50 (2018) 72.
[20] E.E.D.R., Othman, D. Hornung, H.T. Salem, E.A. Khalifa, T.H. El-Metwally, and A. Al-Hendy, European Journal of Obstetrics & Gynecology and Reproductive Biology 137 (2008) 240.
[21] J. Jiang, Z. Jiang, M. Xue, Gynecological Endocrinology 35 (2019) 571.
[22] J. Suen, Y. Chang, P. Chiu, T. Hsieh, E. Hsi, Y. Chen, Y. Chen, and E. Tsai, The American Journal of Pathology 184 (2014) 464.
[23] A. Nanda, K. Thangapandi, P. Banerjee, M. Dutta, T. Wangdi, P. Sharma, K. Chaudhury, and S.K. Jana, Annals of Laboratory Medicine. 40 (2020) 390.
[24] L. Della Corte, C. Di Filippo, O. Gabrielli, S. Reppuccia, V.L. La Rosa, R. Ragusa, M. Fichera, E. Commodari, G. Bifulco, and P. Giampaolino, International Journal of Environmental Research and Public Health 17 (2020) 4683.
[25] G. Jones, C. Jenkinson, and S. Kennedy, Journal of Psychosomatic Obstetrics & Gynecology 25 (2004) 123.
[26] L. Li, C. Cheng, H. Yang, H. Ye, X. Luo, and M. Xi, Acta Physica Polonica A 138 (2020) 338.

[27] X. Zhang, S. Liu, J. Pan, H. Jia, Z. Chen, and T. Guo, Analytical and Bioanalytical Chemistry 411 (2019) 3941.
[28] J. Zhou, N. Gan, T. Li, H. Zhou, X. Li, Y. Cao, and F. Hu, Sensors and Actuators B 178 (2013) 494.
[29] E. Makhneva, Z. Farka, M. Pastucha, A. Obrusník, V. Horáčková, P. Skládal, and L. Zajíčková, Analytical and Bioanalytical Chemistry 411 (2019) 7689.
[30] S. Nootchanat, W. Jaikeandee, P. Yaiwong, C. Lertvachirapaiboon, K. Shinbo, K. Kato, and A. Baba, ACS Applied Materials & Interfaces 11(2019) 11954.
[31] N. Ma, T. Zhang, T. Yan, X. Kuang, H. Wang, D. Wu, and Q. Wei, Biosensors and Bioelectronics 143 (2019) 111608.
[32] K.Y. Goud, V.S. Kumar, A. Hayat, K.V. Gobi, H. Song, K.H. Kim, and J.L. Marty, Journal of Electroanalytical Chemistry 832 (2019) 336.
[33] H. Zhang, Y. Niu, J. Feng, H. Guo, X. Ye, and H. Cui, Fertility and Sterility 86 (2006) 274.
[34] A.S. Browne, J. Yu, R.P. Huang, A.M. Francisco, N. Sidell, and R.N. Taylor, Fertility and Sterility 98 (2012) 713.
[35] S. Shukla, Y. Haldorai, I. Khan, S.M. Kang, C.H. Kwak, S. Gandhi, and Y.K. Han, Materials Science and Engineering 113 (2020) 110916.
[36] T. Kalyani, A. Sangili, A. Nanda, S. Prakash, A. Kaushik, S.K. Jana, Bioelectrochemistry 139 (2021) 107740.
[37] T. Kalyani, A. Nanda, and S.K. Jana, Analytica Chimica Acta 1146 (2021) 146.
[38] A. Sangili, T. Kalyani, S.M. Chen, A. Nanda, and S.K. Jana, ACS Applied Bio Materials. 3 (2020) 7620.
[39] S. Mahari, A. Roberts, and S. Gandhi, Food Chemistry 390 (2022) 133219.
[40] S. Mahari, A. Roberts, D. Shahdeo, and S. Gandhi, BioRxiv. (2020) 059204.
[41] S. Gandhi, I. Banga, P.K. Maurya, and S.A. Eremin, RSC Advances 8 (2018) 1511.
[42] A. Talan, A. Mishra, S.A. Eremin, J. Narang, A. Kumar, and S. Gandhi, Biosensors and Bioelectronics 105 (2018) 14.
[43] S.H. Baek, H.W. Song, S. Lee, J.E. Kim, Y. H. Kim, J.S. Wi, and S.W. Nam, Frontiers in Chemistry. 8 (2020) 285.
[44] A. Baraket, M. Lee, N. Zine, M. Sigaud, J. Bausells, and A. Errachid, Biosensors and Bioelectronics 93 (2017) 170.
[45] M. Lee, N. Zine, A. Baraket, M. Zabala, F. Campabadal, R. Caruso, and A. Errachid, Sensors and Actuators B 175 (2012) 201.
[46] A. Baraket, M. Lee, N. Zine, N. Yaakoubi, M.G. Trivella, M. Zabala, A. Errachid, Procedia Engineering 47 (2012) 1181.
[47] A. Baraket, M. Lee, N. Zine, M. Sigaud, N. Yaakoubi, M.G. Trivella, and A. Errachid, Sensors and Actuators B 189 (2013) 165.

[48] F. Nessark, M. Eissa, A. Baraket, N. Zine, B. Nessark, A. Zouaoui, and A. Errachid, Electroanalysis 32 (2020) 1795.
[49] N. Ruecha, K. Shin, O. Chailapakul, and N. Rodthongkum, Sensors and Actuators B 279 (2019) 298.
[50] P. Razmshoar, S.H. Bahrami, M. Rabiee, I.A. Frias, M. Hangouet, M. Martin, and N. Jaffrezic-Renault, Journal of Electroanalytical Chemistry 926 (2022) 116953.
[51] T. Kalyani, A. Sangili, H. Kotal, A. Kaushik, K. Chaudhury, and S.K. Jana, Biosensors and Bioelectronics: X 14 (2023) 100353.